Energy 257 (2022) 124799

Contents lists available at ScienceDirect

Energy

journal homepage: www.elsevier.com/locate/energy

Experimental and numerical Investigation on the design of a bioinspired PEM fuel cell

Christian Suárez [a, b, *], Alfredo Iranzo [a], Baltasar Toharias [a], Felipe Rosa [a]

[a] Thermal Engineering Group, Energy Engineering Department, School of Engineering, University of Seville, Spain
[b] AICIA, Andalusian Association for Research & Industrial Cooperation, Seville, Spain

ARTICLE INFO

Article history:
Received 5 April 2022
Received in revised form
8 July 2022
Accepted 10 July 2022
Available online 12 July 2022

Keywords:
Polymer electrolyte membrane fuel cell
Biomimetics
Flow field design

ABSTRACT

Proton exchange membrane fuel cells (PEMFCs) are promising energy devices that directly convert chemical energy of fuels such as hydrogen to useful work with negligible environmental impact and high efficiency. The channel geometry of the Bipolar Plate (BP) has a considerably impact on the PEMFC performance. BP designs based on nature-inspired structures such as leaves, lungs or sponges have been explored to date with success but have not yet achieved their full potential. With the objective of researching new flow field designs with enhanced operation, this work presents an experimental analysis of a novel bioinspired design of the channels of a PEMFC. Starting from a CFD fluid flow analysis of different novel initial biomimetic designs, the most promising one was selected, manufactured and tested experimentally. Experimental results comprise polarization and power curves for a comprehensive set of operating conditions. Results were analysed and compared against a reference parallel-serpentine model. Results indicated that the proposed novel biomimetic design is particularly suited for improving water management at high reactants humidity reaching out a peak power a 6.0% higher in comparison with the reference design. Future research should further develop novel design variants and analyze water distribution within the channels.

© 2022 The Authors. Published by Elsevier Ltd. This is an open access article under the CC BY-NC-ND license (http://creativecommons.org/licenses/by-nc-nd/4.0/).

1. Introduction

Biomimicry or biomimetics, derived from the Greek words bio (life) and mimesis (imitation), can be defined as a new science that studies nature's models and then imitates or takes inspiration from these designs and processes to solve human problems [1].

Due to the complexity and heterogeneity of biological systems, the number of features that might be imitated is large and thus Biomimicry could in principle be applied in many fields. Taking the example of plants, leaf veins systems form an integrated network responsible for water, nutrient, and sugar transport, that has been optimized according to evolution via natural selection in terms of simplicity, durability and efficiency. Other similar examples of biological transport systems of interest include lungs or sponges. By analogy with such biological systems, one of the functions of Bipolar Plates in Polymer Electrolyte Membrane Fuel Cells (PEMFCs) is to distribute reactants and evacuate waste products (Fig. 1).

Bipolar Plates are key components for ensuring an appropriate water management within the cell, preventing flooding and enhancing the cell operation at high current densities [2,3]. A properly optimized flow design allows the fuel cell to develop uniform and stable power output and correctly manage spin-off water from the reaction [4]. The design of the flow channels may vary; they may be linear, serpentine, parallel, comb-like or evenly spaced [5]. Each flow field design has its advantages and disadvantages in terms of distribution and pressure drop of the reactants, maximum speeds in channels, ease of dragging of the water product, contact surface with the Gas Diffusion Layer to facilitate the conduction of electrons, among others. In addition, with each of the different configurations, the section of the channels and their dimensions can be modified, and consequently there are numerous design variables that influence the final performance [6]. A contribution in this matter was analysed by Heck et al. [7], who studied the relative effects of pressure and distribution characteristics in traditional serpentine and parallel flow fields designs on a fuel cell unit and proposed a method of decoupling these effects. They obtained a 17% better performance of the serpentine

* Corresponding author. Thermal Engineering Group, Energy Engineering Department, School of Engineering, University of Seville, Camino de los Descubrimientos s/n. 41092 Seville, Spain.
E-mail address: christian.suarez@aicia.es (C. Suárez).

https://doi.org/10.1016/j.energy.2022.124799
0360-5442/© 2022 The Authors. Published by Elsevier Ltd. This is an open access article under the CC BY-NC-ND license (http://creativecommons.org/licenses/by-nc-nd/4.0/).

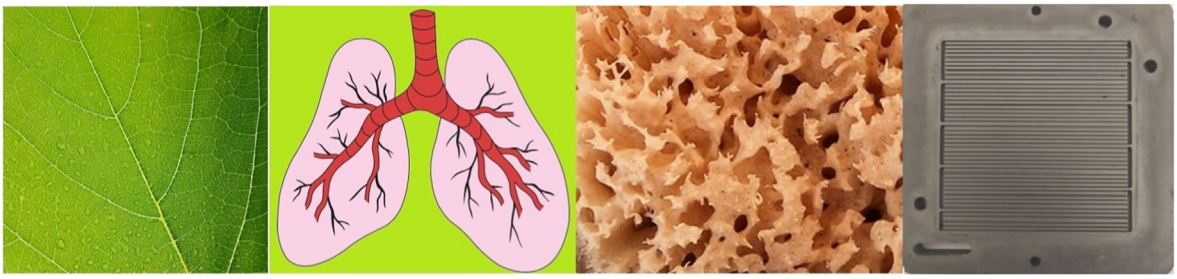

Fig. 1. Analogy of different biological structures with transport and distribution of fluids and PEMFCs.

design and conclude that the major contribution was due to mass transport effects (12%), while the rest (5%) was due to the effect of increased pressure loss.

There has been an increasing trend aiming at recreating nature-inspired bipolar plates with higher performance [2] and several numerical and experimental works can be found in the literature including bioinspired designs by leaves, lungs, or sponges among others.

Leaves have been used as inspiration for a wide variety of designs and works. Several research works can be found in the literature with numerical results that predict advantages in the new leaves-inspired designs in comparison with conventional designs, in terms of overall pressure drop and homogeneity velocity distributions throughout the flow channels [8–11], water removal [12] or cell performance improvement [9,10]. Some experimental results also corroborate the potential of BP designs bioinspired by leaves. Kloess et al. [13] experimental studies obtained an increment up to 30% in peak power, Saripella et al. [14] experiments revealed improved water management and fuel cell performance characteristics and, more recently, Kahraman and Coban [15] observed a performance improvement up to 42.1% in comparison with the standard serpentine design.

Concerning BP bioinspired designs by lungs, Kloess et al. [13] numerical and experimental results also found that lower pressure drop, as well as a more uniform gas distribution when compared to conventional serpentine designs. Ozden et al. [16] studied three different designs bioinspired by lungs and concluded that all of the bioinspired flow fields demonstrated their highest performance when used on the cathode. However, even though with their best flow field configuration the peak power density was higher than the conventional serpentine design, results in general did not demonstrate a significant improvement in performance. Asadzade et al. [17] studied a novel bipolar plate based on lung-shaped bio-inspired flow pattern throughout CFD simulations and obtained better results in terms of the polarization curve and power density curve with respect to the serpentine reference design. Trogadas et al. [18] applied the fractal geometry of the lung to overcome reactant homogeneity issues and also obtained experimentally a performance improvement with respect to a conventional serpentine flow field. Further experiments were carried out for the lung-inspired design by means of Neutron Radiography [19], in order to assess the liquid water content and distributions for different relative humidity values.

Less works can be found in the literature regarding sponges bioinspired designs. Karthikeyan et al. [20] investigated the influence of 2 mm porous carbon inserts in different channel designs and found that the zig flow field pattern with porous carbon inserts produced higher current density compared to others. They also found that, by the capillary action of porous inserts, water accumulated at cathode was removed. More recently, Karthikeyan et al. [21] experimentally studied two types of porous inserts namely porous carbon inserts and porous sponge inserts, and obtained a better performance due to water removal. They also found that porous sponge inserts had increased performance compared to porous carbon inserts, and that increasing the size of the porous inserts improved the PEMFC performance. Marappan et al. [22] also experimentally studied diverse porous sponge inserts for various reaction areas of 25, 50 and 100 cm^2. They concluded that the adoption of 4 mm porous sponge inserts with the porosity of 90% on the cathode side of PEMFC using the modified serpentine with staggered provisions of 4 mm porous sponge inserts yields better performance than the standard serpentine design and had a significant effect on reducing the water flooding. In particular, for the modified serpentine with staggered provisions of porous sponge inserts flow field design (MSSFF), they reported an experimental peak power density of 0.298 W/cm^2 reached at a current density of 0.8 A/cm^2 for the reaction area case of 50 cm^2. Other related works include the use of foams as flow distributors to achieve a more evenly distribution of both hydrogen and oxygen from inlet to outlet through the fuel cell [23–25]. In particular, a functionally graded porous material model was developed by Kermani et al. [25] for foam-based flow distributors, reported a 84% and 130% higher performances in comparison to a conventional parallel-serpentine design.

Many other bioinspired flow channel designs different than leaves, lungs or sponges have been also reported in the field of PEMFCs designs, such as honeycomb structures [26,27], fishbone structures [28] or blood vessels structures [29] to cite some of them.

From the above literature review, it is clear that the use of nature as a source of inspiration for new innovative designs of bipolar plates can potentially produce a better performance of the fuel cell in comparison with the standard parallel or serpentine designs [7,13,15,25]. A critical review of the performance improvement obtained with biomimetic designs shows that in the majority of cases the biomimetic designs present higher cell voltages and more efficient water management with respect to the conventional designs. In particular, leaf and lung-based designs have shown the most promising improvements in terms of performance [2]. However, due to the complexity of the physical and electrochemical phenomena occurring within fuel cells, the large number of possible bioinspired designs with different geometrical characteristics and the lack of standardization regarding performance benchmarking, biomimetic designs have not yet achieved their full potential and further research is needed.

In the present work new flow channel designs bioinspired by leaves, lungs and sponges with different characteristics were investigated. Firstly, the layouts of three different biomimetic flow fields of own creation were presented. These initial proposed designs were evaluated at an early stage using Computational Fluid Dynamics (CFD) models and simulations, in order to understand and improve the flow characteristics of the reactants in BPs, pressure and velocity fields. Later, the most promising design was

selected for manufacturing and was experimentally tested. Results in terms of the current density and power curves were compared against a standard state-of-the-art parallel-serpentine design, as it is among the most well-documented flow field designs, both computationally and experimentally, and are often used as benchmark designs [6,30–32].

2. Materials and methods

A description of materials and research procedure is described in this section. Starting from three initial conceptual designs, namely A, B and C, four novel final biomimetic designs based on leaves, lungs and sponges were developed for the cathode channel's configuration of a 50 cm^2 active area PEMFC with a channel to rib ratio of 1.

In a first step, for each initial conceptual design, a simplified 3D CFD model of the cathode side was previously conducted. Velocity and pressure distributions of these initial designs were evaluated at an early stage using the corresponding CFD models and simulations. After examining CFD simulation results, geometrical modifications were iteratively made in each initial design to improve flow fields characteristics, obtaining the final designs. In a second step, pressure and velocity flow fields of the final designs were compared, and the most promising design was selected and manufactured. Finally, in a third step, performance experiments of the selected design were carried out in a fuel cell test station and results were compared with the reference case of a conventional parallel-serpentine design for different operating conditions. The steps followed and the research methodology are depicted in Fig. 2. Each research step is detailed in the following sections.

2.1. Step 1: reference parallel-serpentine design and proposed novel biomimetic designs

In a first step, a state-of-the-art parallel-serpentine design and three initial novel biomimetic conceptual designs bioinspired by leaves and lungs were analysed and improved in terms of flow fields characteristics using CFD.

2.1.1. Reference serpentine design description

The reference parallel-serpentine design of 50 cm^2 active area used in this work corresponds to the parallel-serpentine flow field from ElectroChem Inc. With graphite bipolar plates. This was used as a reference to compare the novel biomimetic designs performance. The flow field consists of five-channel serpentine connected by manifolds at the end of each pass (Fig. 3). Air flows from the inlet

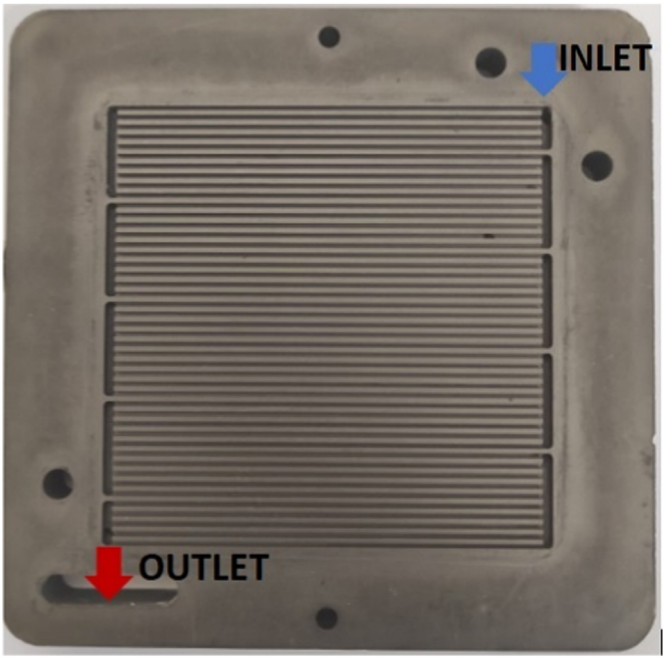

Fig. 3. Reference parallel-serpentine cathode design from ElectroChem Inc.

located at one corner of the BP and is conducted through the serpentine channels to the outlet located at the opposite corner.

2.1.2. Initial biomimetic designs description

The reference parallel-serpentine design and the three novel initial biomimetic design concepts are depicted in Fig. 4, including zoom areas for a better visualization of the geometry details. Regarding the three initial design concepts restrictions and principles, it was kept constant the BP square shape, the inlet and outlet locations in opposite corners and the channel to rib ratio of approximately 1. Symmetry was chosen preferably when appropriate and straight channels with secondary/tertiary branches of smaller section were designed following as a reference Murray's law [33], regarding the third power relation between parent and daughters' diameters. However, too small sections were avoided in the designs to ensure the feasibility of the prototype manufacture. Design A channel's structure, with symmetry with respect to the BP diagonal, consists of a main branch going along the BP diagonal with ramified secondary branches in perpendicular direction,

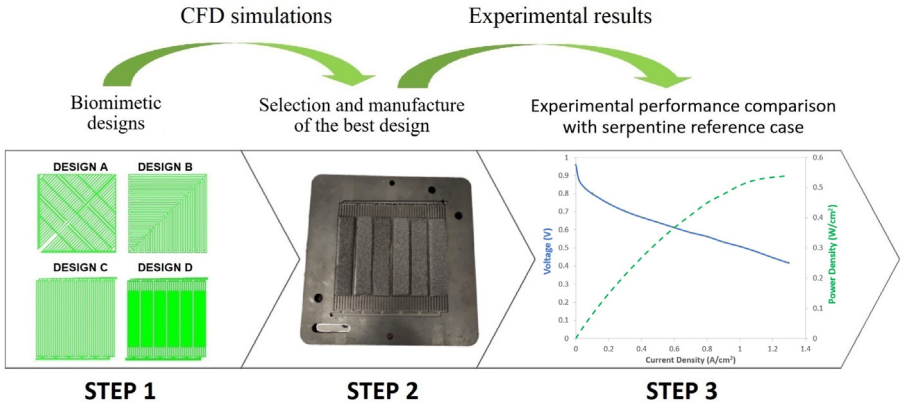

Fig. 2. Global research methodology.

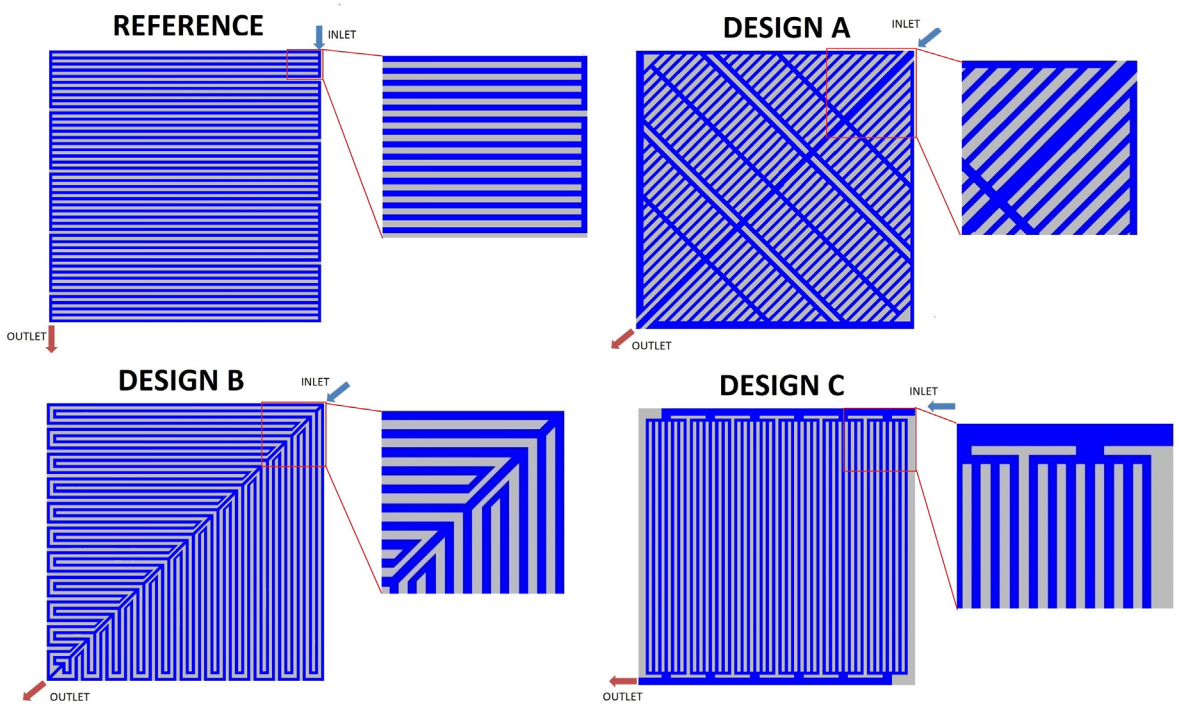

Fig. 4. Reference parallel-serpentine design and initial biomimetic design concepts.

which at the same time are connected throughout tertiary perpendicular branches. In design B, channel layouts consist of a double serpentine flow channel. Its flow path is continuous from inlet to outlet and there is geometrical symmetry with respect to the main BP diagonal. Initial design C consists of an inlet collector and an outlet collector connected in parallel with 6 groups of straight channels in sets of 7 channels each (the total number of vertical channels is 42). Six derivations from the inlet collector and the outlet collector were considered (one for each group).

2.1.3. CFD model description and improved final designs

A simplified 3D CFD model of the cathode fluid flow, including the channels geometry and the gas diffusion layer (GDL), was performed for the parallel-serpentine reference case and the three novel bioinspired designs. The objective of the simplified 3D CFD model was to evaluate at an early stage the fluid flow (velocity and pressure distributions) of the proposed initial designs and some of their different geometry variants with lower computational cost in comparison to consider the whole fuel cell including the electrochemical model.

A sketch of the CFD model geometry and boundary conditions (BCs) is included in Fig. 5(a) for the parallel-serpentine reference case. Channels width and depth dimensions were set to 0.8 mm and 1.1 mm respectively. GDL depth was set to 0.42 mm and modelled as a porous media with a permeability of $4 \cdot 10^{-12}$ m^2. The channel to rib ratio was set to a value of approximately 1.

Representative BCs for operating conditions of a current density of 1 A/cm^2 and a cathode stoichiometry of 2.5 were adopted in the model through a mass flow rate supply of air of $5.03 \cdot 10^{-5}$ kg/s at the inlet and a uniform consumption of air of $4.15 \cdot 10^{-6}$ kg/s in the GDL external surface (corresponding to the GDL-cathode electrode interface). For the outlet, a zero average static pressure outlet BC was applied.

The mesh, considering both channels and GDL layers, was generated using ANSYS ICEM software. A hexahedral mesh was created, and a mesh independence analysis was performed on it,

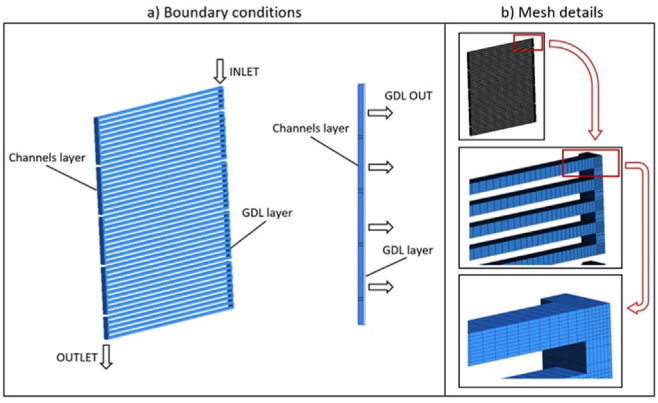

Fig. 5. (a) Parallel-serpentine CFD model geometry and BCs and (b) mesh details.

selecting a mesh with 1.35 million nodes and 0.37 million elements with a mesh quality in the range 0.95–1.0 for the 100% of elements. An illustration including different zoom areas of the mesh details is presented in Fig. 5(b). These same BC's and similar mesh characteristics were kept fixed for the rest of the CFD models of the novel bioinspired designs.

CFD simulations of the reference design and the initial design concepts were performed with ANSYS CFX software and conservation equations for mass and momentum were solved using a high-resolution advection scheme. Laminar flow and steady-state were assumed in the simulations and results were analysed in terms of velocity flow fields and pressure. CFD results provide useful information regarding the mass flow distribution within the different channels and the values of higher and lower velocities, pressure distribution and total pressure drop. An illustrative example of CFD results for the reference parallel-serpentine design is shown in Fig. 6, including velocity and pressure distributions within the channels.

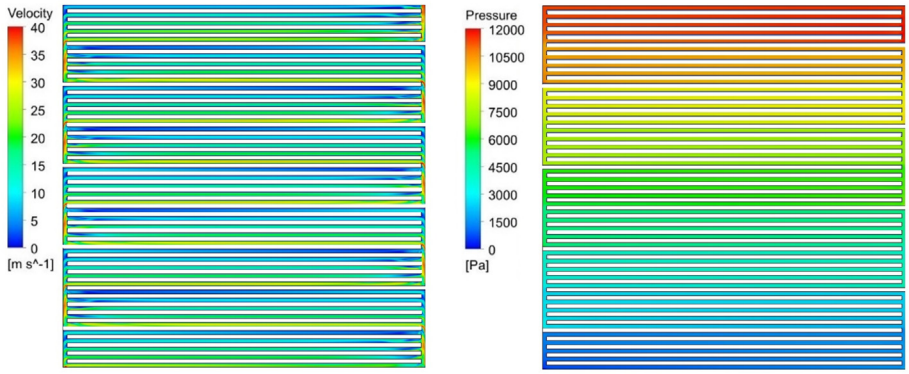

Fig. 6. CFD results of parallel-serpentine design (a) Velocity distribution, (b) Pressure distribution.

Starting from the novel initial biomimetic designs (A, B and C), modifications were iteratively made in the channels' geometry after examining CFD simulations results, improving uniformity in the velocities, avoiding recirculation zones of very low velocities, and also analysing pressure drop. In this way, in each design iteration, the geometry is modified obtaining a more uniform reactant distribution.

The obtained final biomimetics designs concepts namely A′, B′, C1′ and C2′, are shown in Fig. 7, with indications of the geometrical modifications with respect to the initial design concepts. Final design A′ was a variant of initial design A with three geometrical modifications: (i) the last part of the main branch going along the BP diagonal is eliminated to prevent preferent flow paths, (ii) four secondary branches ramified in perpendicular direction of the main branch which had low mass flow rates were also eliminated to obtain a better fluid flow distribution and (iii) a decreasingly variable thickness was set to the main branch to improve fluid flow distribution. Final design B′ had the same geometry as initial design

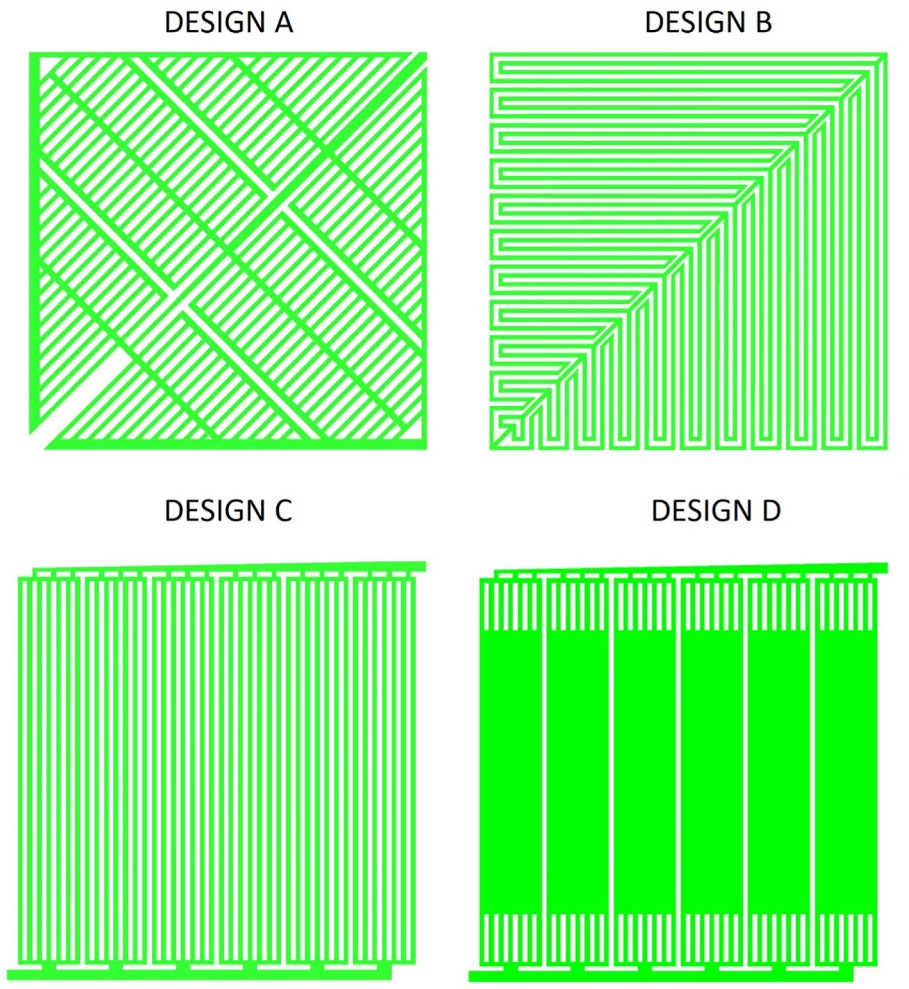

Fig. 7. Final biomimetic designs concepts.

B, as the double serpentine geometry in the channels guarantees a uniform flow mass distribution. Two final designs, namely C1′ and C2′ were obtained starting from initial design concept C. In design C1′ two modifications were included to improve fluid flow distribution: (i) two additional derivations from the inlet collector for each of the six groups were added and (ii) a decreasingly variable thickness was set to the inlet collector. In design C2' an additional modification was included (iii) substituting the central part of the vertical channels of each of the six groups for porous sponge inserts.

2.2. Step 2: selection and manufacture of the best alternative

A comparison of the reference design and the final biomimetic designs in terms of flow velocity and pressure drop CFD simulation results is presented and discussed in the results section. The most promising design C2' was selected and the BP with the proposed channels layout was manufactured with graphite as material base as shown in Fig. 8 (left). Graphene porous sponge inserts (density of 320 mg/cm^3 and pore size of 580 μm) from Graphene Supermarket (Ronkonkoma, NY, USA) were located at each of the central part of the six groups that connect the inlet and the outlet collectors. A computed tomography of the graphene foam is shown in Fig. 8 (right).

2.3. Step 3: experimental performance comparison with parallel-serpentine design

2.3.1. Fuel cell test station description

The experimental work was conducted with a PEM fuel cell test station, devoted to the experimental testing of PEM single cells and short stacks up to 500 W. The test environment, as shown in Fig. 9 (left), is the typical of a fuel cell test bench, with a reactant gas handling unit including humidifiers and back-f regulators, a PID-controlled cell heating/cooling system based on film heaters and air fans, and an electronic load. A sketch of the P&ID is included in Fig. 9 (right).

2.3.2. Experimental procedure and tested operating conditions

The I–V polarization curves and its corresponding power curves were obtained for the cell by following the experimental methodology defined in the well stablished FCTESTNET [34] and FCTESTQA [35] procedures for single cells. Each test started with a preconditioning of the fuel cell, in which the corresponding operating conditions were stablished to their specific values. During the stabilization of the conditions, the current density was increased by steps of 100 mA/cm^2 for the given fixed values of temperature and gas conditions, while keeping the cell voltage higher than 500 mV until reaching the initial reference IV point identified for the conditioning (500 mA/cm^2). Then, the cell was maintained at 500 mA/

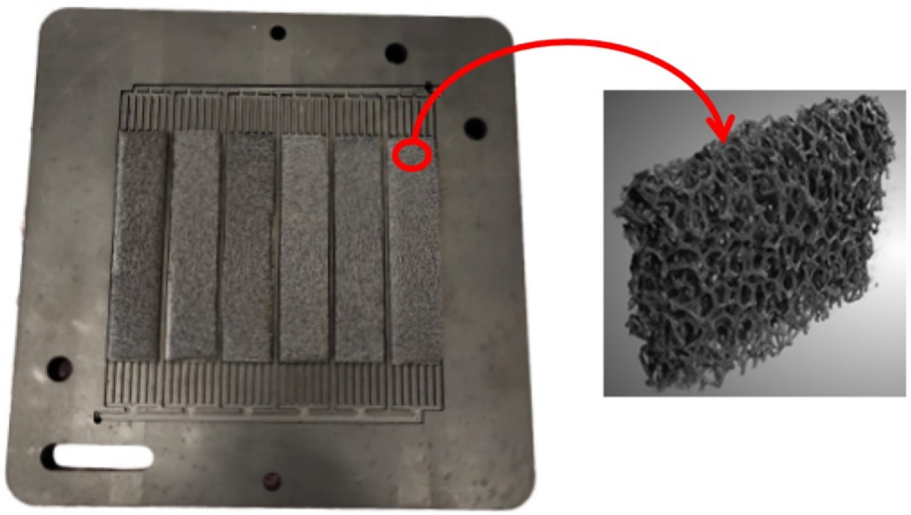

Fig. 8. Manufactured design C2' (left) and detail of computed tomography of graphene foam (right).

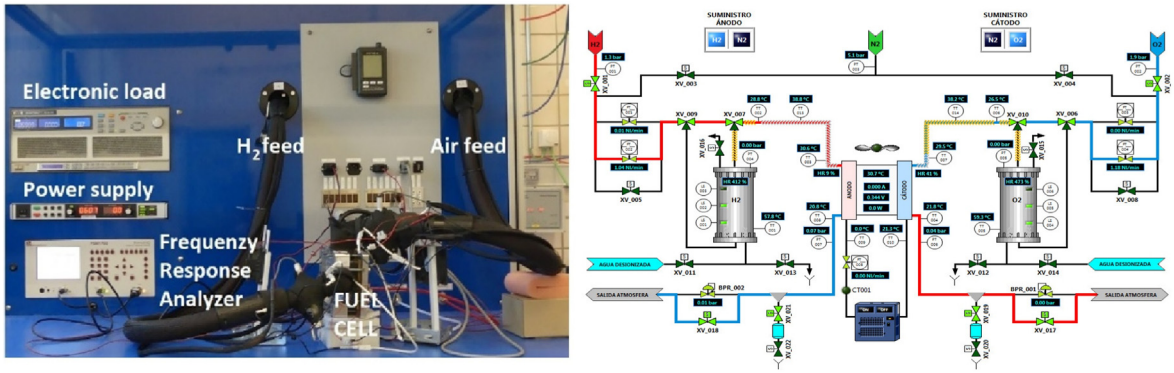

Fig. 9. Fuel cell test station (left) and P&ID (right).

cm^2 during 20 min and the corresponding cell voltage was measured and used as an initial reference IV point. After that, the cell voltage was brought to OCV for a fixed period allowing the stabilization of the operating conditions. Finally, the measurement of the current-voltage curves is carried out in galvanostatic mode, starting at the open circuit voltage, and using fixed current steps. The dwell time for each current density set point is set to 20 min (15 min for conditions stabilization and 5 min for data acquisition).

A comprehensive set of operating conditions was used to analyze the effect of the different conditions of the cell performance. In each operating condition, as shown in Table 1, the following variables are fixed: cell pressure, cell temperature, anode and cathode relative humidity and anode and cathode stoichiometric factor. Initially, a benchmark case using air as oxidant of operating conditions in the cell of 0.5 bar, 65 °C and 60% for cell pressure, cell temperature and relative humidity in anode and cathode respectively was defined. Stoichiometric factors at anode and cathode were fixed to 1.3 and 2.5 respectively. The rest of operating conditions were defined by modifying one of the parameters of the benchmark case. A total of six operating conditions were tested, where it can be observed that two pressure conditions were analysed (0.5 and 1.0 bar), three temperature conditions (55, 65 and 75 °C), two RH conditions (60 and 90%) and two values of the cathode stoichiometric factor (2.5 and 3.5). The different operating conditions were named referencing sequentially the cell pressure, the cell temperature, the anode stoichiometric factor, the anode relative humidity, the cathode stoichiometric factor, the cathode relative humidity and the oxidant (air). As an illustrative example of the nomenclature used in this work, the benchmark case was named as "P05_T65_a13RH60_c25RH60_air". In Table 1 the tested operating conditions are shown and named according to the nomenclature described above, marking in bold the condition varied in each case with respect to the benchmark conditions.

3. Results

In this section, CFD simulation results of the final biomimetic design candidates A′, B′, C1′ and C2' were firstly included, and an analysis of velocity and pressure flow fields was performed to select the most promising alternative. Finally, the selected design was manufactured and experimentally tested for a comprehensive set of operating conditions.

3.1. Final biomimetic designs CFD simulation results

Velocity contours and vectors of the final biomimetic design

Table 1
Operating conditions defined in the experimental tests.

Case	Pressure (bar)	Temperature (°C)	RH (%)	λa	λc
P05_T65_a13RH60_c25RH60_air	0.5	65	60	1.3	2.5
P10_T65_a13RH60_c25RH60_air	**1.0**	65	60	1.3	2.5
P05_T55_a13RH60_c25RH60_air	0.5	**55**	60	1.3	2.5
P05_T75_a13RH60_c25RH60_air	0.5	**75**	60	1.3	2.5
P05_T65_a13RH90_c25RH90_air	0.5	65	**90**	1.3	2.5
P05_T65_a13RH60_c35RH60_air	0.5	65	60	1.3	**3.5**

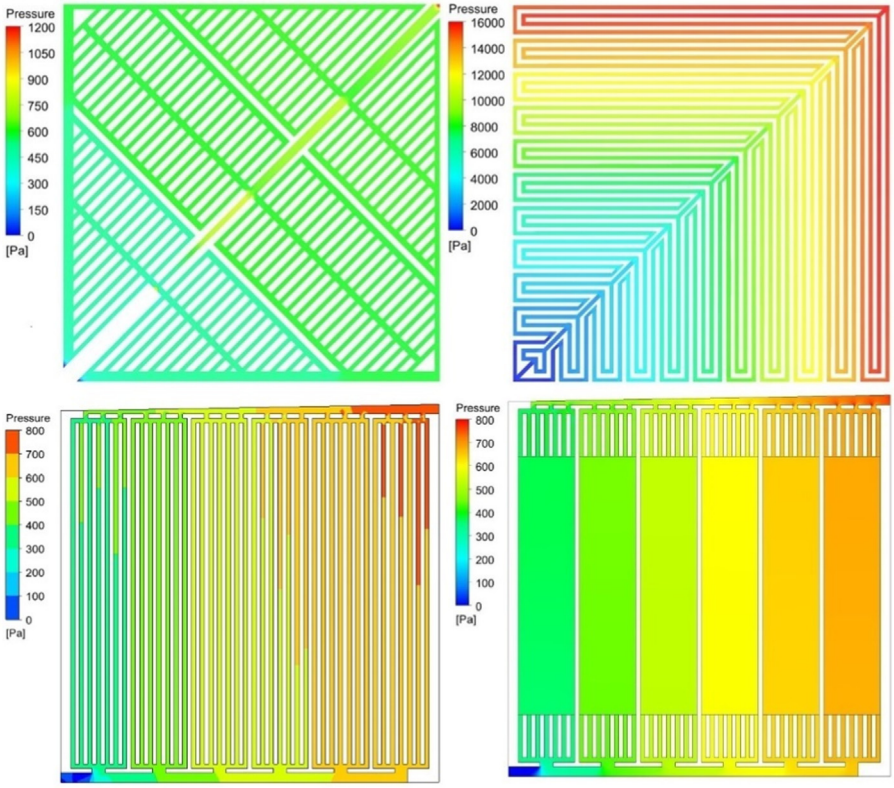

Fig. 10. Velocity flow field of final biomimetic designs A′, B′, C1′ and C2′.

Table 2
Velocity quantitative results of final biomimetic designs A′, B′, C1′ and C2'.

Velocity	Design A′	Design B′	Design C1′	Design C2′
v_{avg} (m/s)	2.29	12.50	2.40	1.71
v_{sd} (m/s)	5.28	12.27	4.51	2.87

Table 3
Pressure quantitative results of final biomimetic designs A′, B′, C1′ and C2'.

Pressure	Design A′	Design B′	Design C1′	Design C2′
Pressure drop (Pa)	2333.3	17851.2	1074.8	1042.8
P_{avg} (Pa)	575.3	9959.4	546.3	537.8
P_{sd} (Pa)	56.6	4162.8	117.5	127.7

candidates A′, B′, C1′ and C2′are shown in Fig. 10 and quantitative results of average velocity and standard deviation velocity are shown in Table 2.

The double serpentine design B′ showed the highest average and standard deviation velocities, with values in the order of 5.2–7.3 times higher in comparison to the other designs A′, C1′ and C2'. Design A′ and C1′ had similar average velocities in the range of 2.29 and 2.40 m/s while standard deviation velocity of design C1′ was lower than design A'. Design C2' showed the most homogeneous velocity flow field, with lower values of the average velocity (1.71 m/s) and standard deviation velocity (2.87 m/s).

Pressure contours of the final biomimetic design candidates A′, B′, C1′ and C2′are shown in Fig. 11 and quantitative results of pressure drop, average pressure and standard deviation pressure are shown in Table 3.

The double serpentine design B′ had the highest pressure drop, with values in the order of 7.6–17.1 times higher in comparison to the other designs A′, C1′ and C2'. Design A′ was the second with higher pressure drop, 2.2 times higher than designs C1′ and C2′, which showed similar values, being C2' the design with the lower pressure drop of 1042.8 Pa.

From the above-described results, design C2' was selected for manufacture as it showed better behaviour in terms of velocities homogeneity and lower values of pressure drop.

3.2. Experimental results and discussion

The selected bioinspired design C2' was manufactured and tested. Experimental diagnostics can help to understand the highly coupled and complex phenomena occurring within a fuel cell, where the polarization curve is the most common measurement of the performance of a fuel cell [36]. The polarization curves and the I–P power curves were obtained for all operating conditions described in Table 1 and results are discussed in this section. Parallel-serpentine design experimental curves obtained from a previous work [30] were also included to serve as a reference for each operating conditions. Operating conditions were grouped in three different sets for the sake of clarity and to account for the effects of anode and cathode relative humidity, cell temperature, and other parameters that include the cell pressure and the cathode stoichiometric factor. Also, the experimental results reported by Marappan et al. [22] for the modified serpentine with staggered provisions of porous sponge inserts flow field (MSSFF) design for the case of the same active area of 50 cm^2 were considered as a reference, even though the operating conditions used in those experiments were different.

The effect of anode and cathode relative humidity is depicted in Fig. 12. The increase in the reactant relative humidity is having a positive effect on the cell performance for the proposed biomimetic

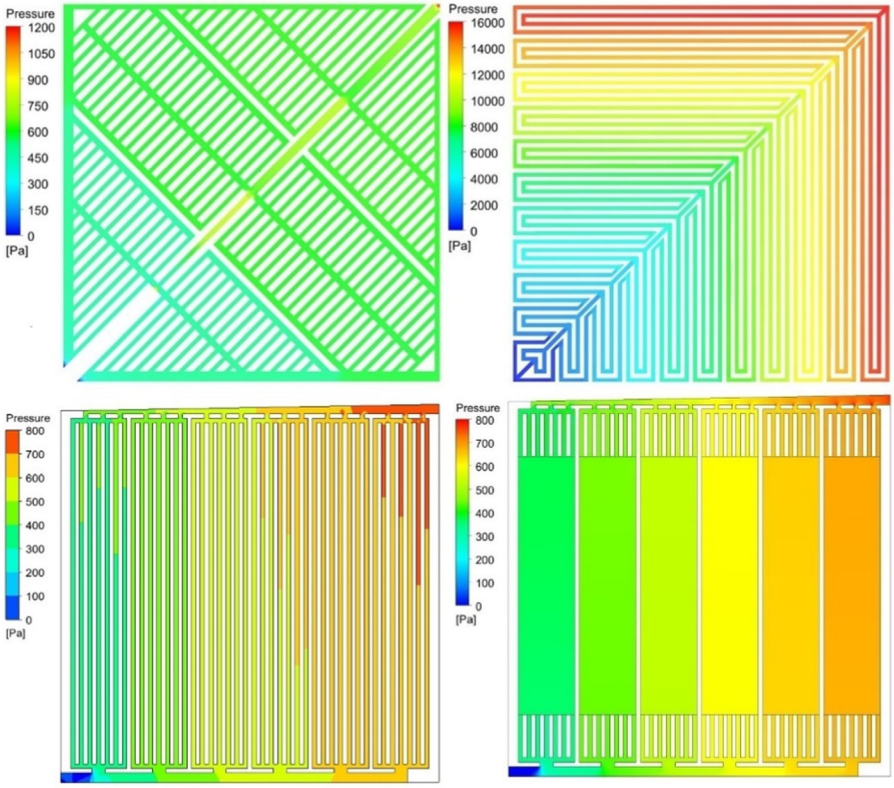

Fig. 11. Pressure contours of final biomimetic designs A′, B′, C1′ and C2′.

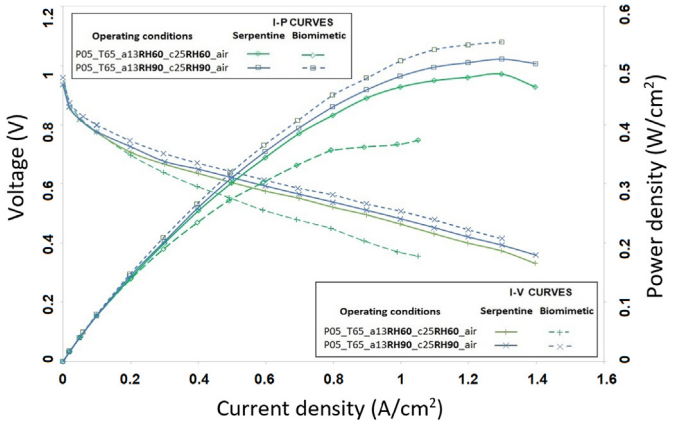

Fig. 12. IV and IP curves for parallel-serpentine and Biomimetic design. Effect of anode and cathode relative humidity.

design, in concordance with the results of the parallel-serpentine design reported by Iranzo et al. [30]. For the parallel-serpentine design, the cell voltage is increasing 25 mV from the reference conditions RH 60% (0.464 V) to RH 90% (0.489 V) at 1.0 A/cm^2, consistently with the increasing cell voltage of the proposed biomimetic design of 130 mV from RH 60% (0.381 V) to RH 90% (0.511 V) at the same current density. The best curve in terms of performance is the one corresponding to the proposed biomimetic design at higher RH values of 90%, reaching out a peak power of 27.2 W, a 6.2% higher in comparison to the 25.6 W of the parallel-serpentine reference and a 82.6% higher in comparison to the 14.9 W reported by Marappan et al. [22] for the modified serpentine with staggered provisions of porous sponge inserts flow field design (MSSFF). This result indicates that the novel biomimetic design is particularly suited for improved water management at high reactants humidity.

The effect of cell temperature is depicted in Fig. 13. The decrease in the cell temperature produces a positive effect on the cell performance for the biomimetic design, in agreement with the results of the parallel-serpentine design reported by Iranzo et al. [30]. For the serpentine design, the cell voltage is increasing 12 mV from the reference cell temperature of 65 °C (0.463 V) to the lower temperature of 55 °C (0.475 V) at 1.0 A/cm^2, consistently with the increasing cell voltage of the proposed biomimetic design of 87 mV from 65 °C (0.381 V) to 55 °C (0.468 V) at the same current density. The peak power of the proposed biomimetic design at a cell temperature of 55 °C was 24.2 W, only a 4.1% lower in comparison to the 25.2 W of the parallel-serpentine reference but a 62.46% higher in comparison to the MSSFF design reported by Marappan et al. [22].

However, for the particular case of the lower temperature of 55 °C, at current densities below 0.5 A/cm^2 the proposed design showed a slightly better performance in comparison with the parallel-serpentine reference. At high cell temperatures (75 °C) the cell performance of both designs is significantly lower indicating a dry-out of the membrane, especially in the biomimetic design, in which, even at low current densities the cell water production was very low and unable to sufficiently hydrate the membrane, and thus only a maximum value of 0.6 A/cm^2 of intensity was reached during the experiments.

The effect of increasing the cell backpressure and increasing the cathode stoichiometric factor is illustrated in Fig. 14. The increase in the cell backpressure produces a positive effect on the cell performance of the biomimetic design, in concordance with the consequent reduction on activation and mass transport losses [31,32] and the results reported for the parallel-serpentine design by Ref. [30]. For the parallel-serpentine design, the cell voltage is increasing 59 mV from a cell backpressure of 0.5 bar (0.463 V) to 1.0 bar (0.522 V) at 1.0 A/cm^2, consistently with the increasing cell voltage of the proposed biomimetic design of 119 mV from 0.5 bar (0.381 V) to 1.0 bar (0.500 V) at the same current density. The peak power of the proposed biomimetic design at a cell backpressure of 1.0 bar was 27.5 W, a 6.2% lower in comparison to the 29.4 W of the parallel-serpentine reference but a 84.6% higher in comparison to the MSSFF design reported by Marappan et al. [22]. However, at current densities below 0.5 A/cm^2 the proposed design at a cell backpressure of 1.0 bar showed a similar performance in comparison with the parallel-serpentine reference with negligible differences.

With respect to the increase in the cathode stoichiometric factor, even though for low current densities performance curves were very similar, for values higher than 0.8 A/cm^2, a better performance of the cell performance for the biomimetic design was observed, consistently with the results reported for the parallel-serpentine design reported by Ref. [30]. For the parallel-serpentine design, the cell voltage is increasing 18 mV from a cathode stoichiometric factor of 2.5 (0.463 V) to 3.5 (0.481 V) at 1.0 A/cm^2, consistently with the increasing cell voltage of the proposed biomimetic design of 20 mV from 2.5 (0.381 V) to 3.5 (0.401 V) at the same current density. The peak power of the proposed biomimetic design at a cathode stoichiometric factor of 3.5 was 20.4 W, a 21.2% lower in

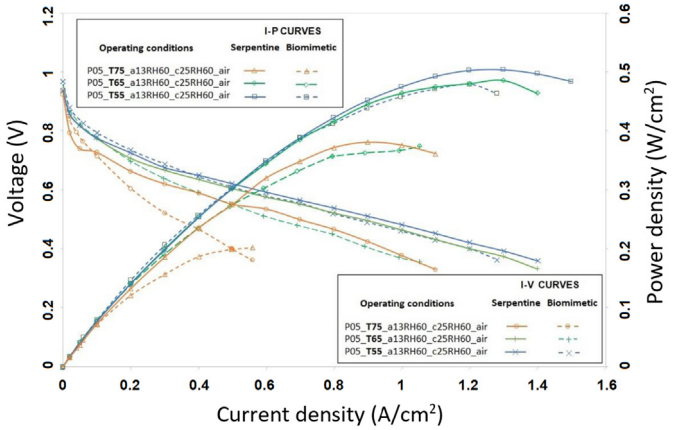

Fig. 13. IV and IP curves for Parallel-serpentine and Biomimetic design. Effect of cell temperature.

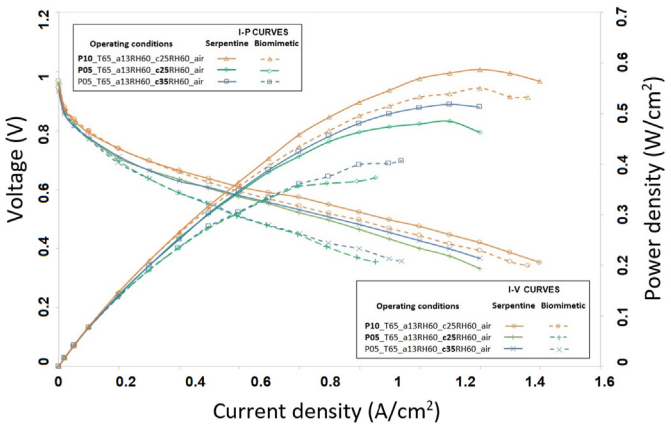

Fig. 14. IV and IP curves for Parallel-serpentine and Biomimetic design. Effect of cell backpressure and cathode stoichiometric factor.

comparison to the 25.9 W of the parallel-serpentine reference but a 36.9% higher in comparison to the MSSFF design reported by Marappan et al. [22].

Despite the promising enhance in the cell performance of the biomimetic design in comparison to the standard parallel-serpentine for the operating conditions of higher relative humidity, and the peak power improvement in comparison to other biomimetic designs including porous sponge inserts [22], further research is required to improve the performance of the proposed design for the rest of operating conditions. Future studies could fruitfully explore this issue further by analysing water distribution within the channels through CFD simulations and neutron imaging techniques. Also, future research should examine novel design variants including geometrical modifications of the channels and the characteristics of the porous sponge inserts.

4. Conclusions

A novel bioinspired channel geometry of a BP has been designed with the aid of CFD modelling, manufactured and experimentally evaluated and compared with a standard parallel-serpentine design. Starting from four initial biomimetic conceptual designs, CFD simulations were conducted and the results in terms of the velocity and pressure distributions within the cathode side channels were analysed using a simplified 3D CFD model. Design C2′, which included graphene porous sponge inserts, showed the most homogeneous velocity flow field, with lower values of the average velocity (1.71 m/s) and standard deviation velocity (2.87 m/s) and the lower pressure drop 1042.8 Pa. This design was thus selected and manufactured. The performance evaluation of the selected biomimetic design was experimentally conducted in a fuel cell test station for a comprehensive set of operation conditions including variations in cell temperature and cell backpressure, reactants RH and cathode stoichiometry. Polarization curves IV and power curves IP were measured and compared with the reference case of a conventional parallel-serpentine design. Similar trends with the parameters' variations were observed for both designs, obtaining higher performances for higher values of anode and cathode relative humidity, cell backpressure and the cathode stoichiometric factors, and for lower values of cell temperature. Even though lower performance was observed for the biomimetic design in comparison to the parallel-serpentine for lower cell temperatures (4.1% lower), higher cell backpressure (6.2% lower) and higher cathode stoichiometric factor of 3.5 (21.2% lower), the novel biomimetic design showed a better performance when operating at higher RH values of 90%, reaching out a peak power a 6.0% higher, indicating that the proposed novel biomimetic design is particularly suited for improved water management at high reactants humidity.

Credit author statement

Christian Suárez: Data curation; Formal analysis; Investigation; Methodology; Writing – original draft; Writing – review & editing.; **Alfredo Iranzo**: Conceptualization; Formal analysis; Funding acquisition; Investigation; Methodology; Project administration; Supervision; Writing – review & editing.; **Baltasar Toharias**: Data curation; Investigation; Software; Visualization; Writing – review & editing.; **Felipe Rosa**: Funding acquisition; Project administration; Resources; Supervision.

Declaration of competing interest

The authors declare that they have no known competing financial interests or personal relationships that could have appeared to influence the work reported in this paper.

Data availability

Data will be made available on request.

Acknowledgements

Grant PID2019-104441RB-I00 funded by MCIN/AEI/10.13039/501100011033 and grant P20_01231 funded by PAIDI 2020 program by Junta de Andalucía, co-funded with ERDF funds.

References

[1] Cohen YH, Reich Y. Biomimetic design method for innovation and sustainability, vol. 10. Berlin, Germany: Springer; 2016.
[2] Iranzo A, Arredondo CH, Kannan AM, Rosa F. Biomimetic flow fields for proton exchange membrane fuel cells: a review of design trends. Energy 2020;190:116435.
[3] Ijaodola OS, El-Hassan Z, Ogungbemi E, Khatib FN, Wilberforce T, Thompson J, Olabi AG. Energy efficiency improvements by investigating the water flooding management on proton exchange membrane fuel cell (PEMFC). Energy 2019;179:246–67.
[4] Olabi AG, Wilberforce T, Abdelkareem MA. Fuel cell application in the automotive industry and future perspective. Energy 2021;214:118955.
[5] Abderezzak B. Introduction to transfer phenomena in PEM fuel cells. Elsevier; 2018.
[6] Manso AP, Marzo FF, Barranco J, Garikano X, Mujika MG. Influence of geometric parameters of the flow fields on the performance of a PEM fuel cell. A review. Int J Hydrogen Energy 2012;37(20):15256–87.
[7] Heck JD, Vaz WS, Koylu UO, Leu MC. Decoupling pressure and distribution effects of flow fields on polymer electrolyte fuel cell system performance. Sustain Energy Technol Assessments 2019;36:100551.
[8] Arbabi F, Roshandel R, Karimi MG. Numerical modeling of an innovative bipolar plate design based on the leaf venation patterns for PEM fuel cells. Int J Eng 2012;25(3):177–86.
[9] Roshandel R, Arbabi F, Moghaddam GK. Simulation of an innovative flow-field design based on a bio inspired pattern for PEM fuel cells. Renew Energy 2012;41:86–95.
[10] Chen T, Gong SC, Xiao Y. Investigation of bifurcation structure flow field for bipolar plates in PEMFC. Heat Mass Tran 2013;49(2):147–53.
[11] Chen T, Liu S, Yang L. Development of flow field plates based on asymmetric leaf structure for PEM fuel cells. Int J Mater Struct Integr 2017;11(4):229–43.
[12] Chen T, Liu S, Gong S, Wu C. Development of bipolar plates with different flow channel configurations based on plant vein for fuel cell. Int J Energy Res 2013;37(13):1680–8.
[13] Kloess JP, Wang X, Liu J, Shi Z, Guessous L. Investigation of bio-inspired flow channel designs for bipolar plates in proton exchange membrane fuel cells. J Power Sources 2009;188(1):132–40.
[14] Saripella BP, Koylu UO, Leu MC. Experimental and computational evaluation of performance and water management characteristics of a bio-inspired proton exchange membrane fuel cell. J Fuel Cell Sci Technol 2015;12(6).
[15] Kahraman H, Coban A. Performance improvement of a single pem fuel cell using an innovative flow field design methodology. Arabian J Sci Eng 2020;45(7):5143–52.
[16] Ozden A, Ercelik M, Ouellette D, Colpan CO, Ganjehsarabi H, Hamdullahpur F. Designing, modeling and performance investigation of bio-inspired flow field based DMFCs. Int J Hydrogen Energy 2017;42(33):21546–58.
[17] Asadzade M, Shamloo A. Design and simulation of a novel bipolar plate based on lung-shaped bio-inspired flow pattern for PEM fuel cell. Int J Energy Res 2017;41(12):1730–9.
[18] Trogadas P, Cho JIS, Neville TP, Marquis J, Wu B, Brett DJL, Coppens MO. A lung-inspired approach to scalable and robust fuel cell design. Energy Environ Sci 2018;11(1):136–43.
[19] Cho JIS, Neville TP, Trogadas P, Meyer Q, Wu Y, Ziesche R, …, Coppens MO. Visualization of liquid water in a lung-inspired flow-field based polymer electrolyte membrane fuel cell via neutron radiography. Energy 2019;170:14–21.
[20] Karthikeyan P, Vasanth RJ, Muthukumar M. Experimental investigation on uniform and zigzag positioned porous inserts on the rib surface of cathode flow channel for performance enhancement in PEMFC. Int J Hydrogen Energy 2015;40(13):4641–8.
[21] Karthikeyan M, Karthikeyan P, Muthukumar M, Kannan VM, Thanarajan K, Maiyalagan T, …, Jothi VR. Adoption of novel porous inserts in the flow channel of pem fuel cell for the mitigation of cathodic flooding. Int J Hydrogen Energy 2020;45(13):7863–72.
[22] Marappan M, Narayanan R, Manoharan K, Vijayakrishnan MK, Palaniswamy K, Karazhanov S, Sundaram S. Scaling up studies on PEMFC using a modified serpentine flow field incorporating porous sponge inserts to observe water molecules. Molecules 2021;26(2):286.
[23] Afshari E, Mosharaf-Dehkordi M, Rajabian H. An investigation of the PEM fuel cells performance with partially restricted cathode flow channels and metal foam as a flow distributor. Energy 2017;118:705–15.

[24] Carton JG, Olabi AG. Three-dimensional proton exchange membrane fuel cell model: comparison of double channel and open pore cellular foam flow plates. Energy 2017;136:185–95.
[25] Kermani MJ, Moein-Jahromi M, Hasheminasab MR, Ebrahimi F, Wei L, Guo J, Jiang FM. Application of foam-based functionally graded porous material flow-distributor to PEM fuel cells. Energy 2022:124230.
[26] Atyabi SA, Afshari E. Three-dimensional multiphase model of proton exchange membrane fuel cell with honeycomb flow field at the cathode side. J Clean Prod 2019;214:738–48.
[27] Zhang S, Liu S, Xu H, Liu G, Wang K. Performance of proton exchange membrane fuel cells with honeycomb-like flow channel design. Energy 2022;239:122102.
[28] Wang Y, Si C, Qin Y, Wang X, Fan Y, Gao Y. Bio-inspired design of an auxiliary fishbone-shaped cathode flow field pattern for polymer electrolyte membrane fuel cells. Energy Convers Manag 2021;227:113588.
[29] Wang CT, Hu YC, Zheng PL. Novel biometric flow slab design for improvement of PEMFC performance. Appl Energy 2010;87(4):1366–75.
[30] Iranzo A, Navas SJ, Rosa F, Berber MR. Determination of time constants of diffusion and electrochemical processes in polymer electrolyte membrane fuel cells. Energy 2021;221:119833.
[31] Mench MM. Fuel cell engines. John Wiley & Sons; 2008.
[32] Barbir F. PEM fuel cells: theory and practice. Elsevier Academic; 2005.
[33] Murray CD. The physiological principle of minimum work: I. The vascular system and the cost of blood volume. Proc Natl Acad Sci USA 1926;12(3):207–14.
[34] FCTESTNET Test procedures. The fuel cell testing and standarization network. EU FP5 Project ENG2-CT2002-20657, draft vol. 1. 2006. p. 4.
[35] FCTESTQA Test protocol. Testing the voltage and power as function of current density. Polarisation curve for a PEFC single cell. Test Module PEFC SC 5-2. European Commission, Joint Research Centre, Institute for Energy; 2010.
[36] Wu J, Yuan XZ, Wang H, Blanco M, Martin JJ, Zhang J. Diagnostic tools in PEM fuel cell research: Part I Electrochemical techniques. Int J Hydrogen Energy 2008;33(6):1735–46.